International Conference on Unmanned Aircraft Systems (ICUAS'19), Atlanta, GA, USA, June 11-14, 2019

Robust Navigation System for UAVs in GNSS- and Magnetometer-Denied Environments

Pål H. Mathisen* and Thor I. Fossen*
Department of Engineering Cybernetics
Norwegian University of Science and Technology
pal.mathisen@ntnu.no

***Abstract*—Navigating in environments where GNSS- and magnetometer measurements are unreliable can lead to a significant decrease in state estimation accuracy. The use of supplementary measurements, either from optical sensors or otherwise, could enhance the state estimates notably even when at low quality. Using inertial navigation corrected by a multiplicative extended Kalman filter, state estimation is performed on a simulated UAV in motion. This paper has investigated the effect of adding measurements of body-fixed velocity and specific force as reference vectors to the navigation systems of UAVs in GNSS- and magnetometer denied environments. A case study for each of the two measured vectors is performed, and compared to a reference flight without dropout of GNSS or magnetometer, and a flight with dropout, but without any additional aiding sensor.**

***Index Terms*—MEKF, Attitude Estimation, Attitude Parametrization, UAV, Sensor Fusion, Reference Vectors**

I. Introduction

A. Background and Motivation

In the past years, unmanned aerial vehicles (UAVs) have gone from being used mostly for military applications to make their entrance into many commercial applications. Their ability to reach remote places and cover large amount of ground faster and cheaper than their alternatives makes them ideal for outdoor tasks such as search-and-rescue operations, remote sensing of agriculture and power line inspection.

When looking at indoor applications for UAVs, many of the advantages are no longer valid. The main reason for using unmanned vessels for indoor operations is when the operation is either dangerous, repetitive or otherwise unattractive to humans. While ground-based mobile robots is a more stable platform, the superior mobility and reach of a multicopter UAV often makes the aerial option the right choice.

There are however additional issues to flying indoor versus the outside case. Due to attenuation and multipathing of signals [1], the range-based positioning aiding from the global navigation satellite systems (GNSS) is rarely a viable option for high-precision indoor navigation solutions. Other sensors used for increased attitude estimation accuracy like the magnetometer are also unreliable in many indoor environments. Electrical motors or presence of ferromagnetic materials will disrupt the magnetic field, which needs to be known. It is therefore required to find alternative sources for sensor packages that could complement the inertial navigation system (INS). Some Possible alternatives are ultra-wideband (UWB) radio beacons positioning system [2], [3], a system utilizing information from a LIDAR-based SLAM-system [4] or optical tracking of landmarks [5], [6].

Creating a robust navigation system that can operate in most environments is a difficult task, especially on a UAV. While integrating additional sensors will give more versatile, self-contained and accurate navigation, it also increases weight, computational strain and power consumption. The choice of sensory packages is therefore a constant trade-off between different factors.

Of the methods available today for fusing sensor information together, the by far most popular is the indirect Kalman filter [7]. The introduction of the multiplicative extended Kalman filter (MEKF) [8] that uses a 3-dimensional attitude error representation of the unit quaternion improves the properties of the Kalman filter's error covariance matrix. Using the unit constraint to reduce the dimension of the attitude error, it simultaneously solves the problem with the error covariance matrix' rank. Another notable state estimation strategy for sensor fusion is the nonlinear observer (NLO) based on pseudorange measurements, reference vectors and inertial sensors [9], [10]. This observer handles the extended Kalman filter's issue with convergence due to linearization error, by introducing semi-global convergence at the cost of the Kalman filter's optimallity. In [11], the NLO is cascaded into an extended Kalman filter, providing a globally stable estimator combined with local optimallity.

All these applications assumes to have at least position and two reference vectors reliably measured, with GNSS for position measurements, and specific force and the magnetic field being the two reference vectors in most cases. None of them handles the issue where these assumptions are violated, either for a brief period or permanently.

This work was supported by the Centre for Autonomous Marine Operations and Systems under Grant 223254.

*Department of Engineering Cybernetics, Norwegian University of Science and Technology, 7491 Trondheim, Norway

B. Contribution

This paper focuses on estimation of the necessary states to perform operations in GNSS- and magnetometer-denied environments. Without the aiding from the magnetometer reference vector and velocity measurements from GNSS, the attitude estimates, and heading in particular, suffers greatly. The work in this paper investigates the effects of introducing an additional reliable, but low-quality reference vector to the navigation system. It is common knowledge that additional measurements with uncorrelated errors will improve estimation accuracy. The focus will therefore be on comparing several cases with varying availability of measurements.

C. Overview

As the task at hand is the investigate the effects of additional measurements in the case of GNSS and magnetometer dropout, a simulated system of a suitable UAV is created. A vehicle simulator with a controller based on [12] is therefore implemented. The detailed layout of the simulator will not be explained in this work, but is available online[1].

The state estimation is performed by fusing information from inertial- and aiding sensors into an MEKF. The layout of the state estimation system is described in detail in Section II. The aiding measurements used are loosely coupled position- and velocity measurements from UWB/GNSS, and reference vectors from magnetometer, optical cameras and specific force estimates. The reference vectors are described in Section III

The case studies performed simulate situations where some sensors are no longer reliable, and what could be done to decrease the performance drop that accompanies it. The details about the cases and the results are described in Section IV.

D. Notation

The use of $||\cdot||_2$ indicates the Euclidean vector norm, matrices and vectors are indicated by square brackets and uses semicolon or line shifts to separate rows and space or comma to separate columns. The operator $(\cdot)_{\text{norm}}$ is a normalization operator for vectors in $\mathbb{R}^{n\times 1}$ that is defined as

$$(\boldsymbol{a})_{\text{norm}} = \frac{\boldsymbol{a}}{||\boldsymbol{a}||_2}$$

A unit quaternion uses the notation $\boldsymbol{q} = [\eta; \boldsymbol{\epsilon}^T]^T$ where $\eta \in \mathbb{R}$ as the real part and $\boldsymbol{\epsilon} \in \mathbb{R}^3$ as the imaginary vector part, and with the property $||\boldsymbol{q}||_2 \triangleq 1$. The conjugate of a quaternion $\boldsymbol{q}$ is denoted as $\bar{\boldsymbol{q}}$, and its inverse $\boldsymbol{q}^{-1}$ is defined as $\bar{\boldsymbol{q}}/||\boldsymbol{q}||_2^2$. The quaternion product is described in vector form as

$$\boldsymbol{q}_1 \otimes \boldsymbol{q}_2 = \begin{bmatrix} \eta_1\eta_2 - \boldsymbol{\epsilon}_1^\top \boldsymbol{\epsilon}_2 \\ \eta_1\boldsymbol{\epsilon}_2 + \eta_2\boldsymbol{\epsilon}_1 + S(\boldsymbol{\epsilon}_1)\boldsymbol{\epsilon}_2 \end{bmatrix}$$

For a three-dimensional vector $\boldsymbol{x} \in \mathbb{R}^3$, the skew-symmetric matrix $S(\boldsymbol{x})$ with the property $S(\boldsymbol{x})\boldsymbol{v} \triangleq \boldsymbol{x} \times \boldsymbol{v}$ is defined as

$$S(\boldsymbol{x}) := \begin{bmatrix} 0 & -x_3 & x_2 \\ x_3 & 0 & -x_1 \\ -x_2 & x_1 & 0 \end{bmatrix}$$

[1]https://github.com/paalhm/AINS-multicopter-simulator

Matrices like the identity and zero matrix are noted with two subscript dimensions in the fashion $(\cdot)_{n\times m}$. If only one subscript is given, the matrix is square. To simplify notation, the coordinate system decomposition of a vector is given by a superscript, meaning that $\boldsymbol{x}^a$ and $\boldsymbol{x}^b$ is the vector $\boldsymbol{x}$ decomposed in the coordinate systems a and b. To rotate from one coordinate to another, the notation $\boldsymbol{R}_b^a$ represent the rotation of a coordinate frame from system a to system b, or a transformation of a vector in the opposite direction. Similarily, a vector of Euler angles or quaternions, $\boldsymbol{\Theta}$ or $\boldsymbol{q}$ could be given the same notation to indicate that $\boldsymbol{R}(\boldsymbol{q}_b^a)$ or $\boldsymbol{R}(\boldsymbol{\Theta}_b^a)$ equals $\boldsymbol{R}_b^a$

The reference frames in use will be the North-East-Down assumed inertial frame (NED) with its origin at $\boldsymbol{p}(t_0)$, denoted with a superscript $\{n\}$, and the local body-frame with its origin in the vehicle's center of mass, denoted with a superscript $\{b\}$. Since the situation simulated is suppose to take place in a geographically static environment and because the rotations of the NED-system is not noticeable with the present sensory package, the NED-system is assumed inertial and constant.

II. Navigation System Design

The navigation system uses inertial measurement units (IMUs) that measure the vehicle's body-aligned accelerations and angular velocities. These measurements are integrated to give estimates of position, velocity and attitude (PVA). It is a well known issue that such inertial navigation is subject to accumulation of IMU errors over time in the state estimates, either from measurement noise or measurement biases. The common solution is to use complementary sensors that allows for in-flight correction of the errors through sensor fusion, called aided inertial navigation. The sensor fusion is done by the indirect multiplicative Kalman filter described in [8], which separates the estimation into a prediction by the IMU-sensors, and a correction using aiding sensors, as seen in Figure 1.

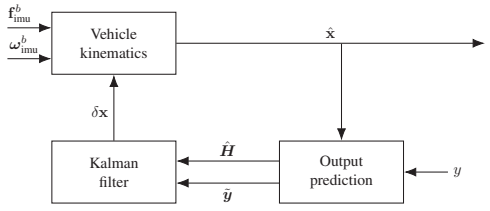

Fig. 1. Block diagram giving an overview of the navigation system. Prediction happens in the Vehicle Kinematics-block, while the corrections happens in the Kalman filter

As the navigation system will estimate the PVA-states, the state vector need to at least contain those states. The state vector $\boldsymbol{x} = [\boldsymbol{p}^{nT}, \boldsymbol{v}^{nT}, \boldsymbol{q}_b^{nT}]^T$ is introduced to simplify notation.

The true vehicle kinematics for PVA is given by

$$\dot{\boldsymbol{p}}^n = \boldsymbol{v}^n \tag{1}$$
$$\dot{\boldsymbol{v}}^n = \boldsymbol{R}_b^n \boldsymbol{f}^b + \boldsymbol{g}^n \tag{2}$$
$$\dot{\boldsymbol{q}}_b^n = \frac{1}{2}\boldsymbol{q}_b^n \otimes \boldsymbol{\omega}_{nb}^b \tag{3}$$

where $\boldsymbol{p} \in \mathbb{R}^3$, $\boldsymbol{v} \in \mathbb{R}^3$, $\boldsymbol{q} \in \mathbb{S}^3$ represents the position, velocity and unit quaternion attitude states respectively, $\boldsymbol{f}$ represents specific force and $\boldsymbol{\omega}_{nb} \in \mathbb{R}^3$ is the angular velocity of $\{b\}$ relative to $\{n\}$.

A. Sensor models

In addition to the IMU sensors, there are several other complementary sensors used for correction of the inertial navigation.

1) Inertial sensors: The inertial sensors models are based on classical strapdown assumptions, i.e that the sensors always measures in the body-fixed frame.

$$\boldsymbol{f}_{imu}^b = \boldsymbol{f}^b + \boldsymbol{b}_a^b + \boldsymbol{w}_a \tag{4}$$
$$\boldsymbol{\omega}_{imu}^b = \boldsymbol{\omega}_{nb}^b + \boldsymbol{b}_g^b + \boldsymbol{w}_g \tag{5}$$
$$\dot{\boldsymbol{b}}_a^b = \boldsymbol{w}_{b,a} \tag{6}$$
$$\dot{\boldsymbol{b}}_g^b = \boldsymbol{w}_{b,g} \tag{7}$$

where $\boldsymbol{b}_i \in \mathbb{R}^3$ for $i \in \{a, g\}$ represents the sensor biases and $\boldsymbol{w}_{b,i} \in \mathbb{R}^3$ is the Gaussian distributed measurement noise. The biases will be discussed later on.

2) Aiding Sensors: The aiding sensors used to correct for errors in the inertial navigation is typically low-rate sensors with lower accuracy, but normally fairly unbiased and complementary to the inertial sensors. This enables the estimation scheme to retain a stable and manageable estimation error.

a) Position measurement sensor: All position measurements are based upon measuring the vehicle's position relative to known objects such as satellites, landmarks or signal beacons. This navigation system focuses on pseudorange-based measurement systems, such as GNSS or UWB beacons. For simplicity, loose integration of the measurements have been modelled, but [10] shows that full observability of translating motions is obtained through three linearly independent line-of-sight vectors.

The position measurement models are as follows

$$\boldsymbol{p}_m^n = \boldsymbol{p}^n + \boldsymbol{v}_p \tag{8}$$

b) Velocity measurements: As GNSS operates on known and stable frequencies, the vehicle velocity in NED frame could be found by measuring the Doppler shift of the signal to find the velocity relative to the satellite [13, Chap. 2].

The velocity measurement model is

$$\boldsymbol{v}_m^n = \boldsymbol{v}^n + \boldsymbol{v}_v \tag{9}$$

Velocity measurements from GNSS will be referred to as VGNSS.

B. Prediction

The prediction step of the navigation system uses the IMU sensor date to predict the new PVA states. The models for the estimation prediction is based upon the vehicle kinematics equations (1)-(3)

$$\dot{\hat{\boldsymbol{p}}}^n = \hat{\boldsymbol{v}}^n \tag{10}$$
$$\dot{\hat{\boldsymbol{v}}}^n = \hat{\boldsymbol{R}}_b^n \hat{\boldsymbol{f}}^b + \boldsymbol{g}^n \tag{11}$$
$$\dot{\hat{\boldsymbol{q}}}_b^n = \frac{1}{2}\hat{\boldsymbol{q}}_b^n \otimes \hat{\boldsymbol{\omega}}_{nb}^b \tag{12}$$

where $\hat{(\cdot)}$ is the estimate of $(\cdot)$ and referred to as the *nominal state*.

If the state vector is augmented with estimates of the IMU-biases, two additional prediction equations are needed, giving

$$\dot{\hat{\boldsymbol{b}}}_a^b = \boldsymbol{0} \tag{13}$$
$$\dot{\hat{\boldsymbol{b}}}_g^b = \boldsymbol{0} \tag{14}$$

This leaves the augmented state vector with the 16 states $\boldsymbol{x} = [\boldsymbol{p}^{nT},\ \boldsymbol{v}^{nT},\ \boldsymbol{b}_a^{bT},\ \boldsymbol{q}_b^{nT},\ \boldsymbol{b}_g^{bT}]^T$

C. Error state dynamics

The indirect Kalman filter operates with error states. There are several advantages with an indirect filter compared with its direct counterpart. For this navigation system, the most important one is that it allows for error states that are not 1-to-1 with the nominal states. This allows for a three-state representation of attitude error, compared to the four needed to represent a unit quaternion. The Gibbs vector is chosen as the attitude error representation [8].

$$\delta\boldsymbol{p}^n = \boldsymbol{p}^n - \hat{\boldsymbol{p}}^n \tag{15}$$
$$\delta\boldsymbol{v}^n = \boldsymbol{v}^n - \hat{\boldsymbol{v}}^n \tag{16}$$
$$\delta\boldsymbol{b}_a^b = \boldsymbol{b}_a^b - \hat{\boldsymbol{b}}_a^b \tag{17}$$
$$\boldsymbol{a}_g = ((\hat{\boldsymbol{q}}_b^n)^{-1} \otimes \boldsymbol{q}_b^n)_{gb} \tag{18}$$
$$\delta\boldsymbol{b}_g^b = \boldsymbol{b}_g^b - \hat{\boldsymbol{b}}_g^b \tag{19}$$

where $\boldsymbol{a}_g \in \mathbb{R}^3$ is the attitude error representation, and the $(\cdot)_{gb}$ operator finds the Gibbs vector of a quaternion through the relationship

$$\boldsymbol{a}_g = (\delta\boldsymbol{q})_{gb} = \frac{\delta\boldsymbol{\epsilon}}{\delta\eta} \tag{20}$$

and inversely, the quaternion reconstruction from a Gibbs vector

$$\delta\boldsymbol{q} = (\boldsymbol{a}_g)_q = \frac{1}{\sqrt{2 + ||\boldsymbol{a}_g||_2^2}} \begin{bmatrix} 2 \\ \boldsymbol{a}_g \end{bmatrix} \tag{21}$$

Using these definitions and combining the equations (1)–(7) and (10)–(14), the resulting error state differential equations are

$$\dot{\delta \boldsymbol{p}}^n = \tilde{\boldsymbol{v}}^n \tag{22}$$

$$\begin{aligned}\dot{\delta \boldsymbol{v}}^n = &-\boldsymbol{R}(\hat{\boldsymbol{q}}_b^n)(\delta \boldsymbol{b}_a^b + \boldsymbol{w}_a) \\ &+ \boldsymbol{R}(\hat{\boldsymbol{q}}_b^n)\boldsymbol{S}(\boldsymbol{a}_g)(\hat{\boldsymbol{f}}^b - \delta \boldsymbol{b}_a^b - \boldsymbol{w}_a)\end{aligned} \tag{23}$$

$$\dot{\delta \boldsymbol{b}}_a^b = \boldsymbol{w}_{b,a} - \frac{1}{T_a}\delta \boldsymbol{b}_a \tag{24}$$

$$\begin{aligned}\dot{\boldsymbol{a}}_g = &-\delta \boldsymbol{b}_g^b - \boldsymbol{S}(\hat{\boldsymbol{\omega}})\boldsymbol{a}_g + \frac{1}{2}\boldsymbol{S}(\delta \boldsymbol{b}_g^b)\boldsymbol{a}_g \\ &- \frac{1}{4}(\delta \boldsymbol{b}_g^b)^T \boldsymbol{a}_g \boldsymbol{a}_g\end{aligned} \tag{25}$$

$$\dot{\delta \boldsymbol{b}}_g^b = \boldsymbol{w}_{b,g} - \frac{1}{T_g}\delta \boldsymbol{b}_g \tag{26}$$

modeling the bias errors as 1st-order Gauss-Markov processes with $T_a > 0$ and $T_g > 0$ being time constants.

As the Kalman filter needs to linearize the differential equation for the error covariance propagation, the matrix $E\left[\frac{d}{d\delta \boldsymbol{x}}\delta \boldsymbol{x}\Big|_{\delta \boldsymbol{x}=\boldsymbol{0}}\right]$ is found to be:

$$\boldsymbol{F} = \begin{bmatrix} \boldsymbol{0}_3 & \boldsymbol{I}_3 & \boldsymbol{0}_3 & \boldsymbol{0}_3 & \boldsymbol{0}_3 \\ \boldsymbol{0}_3 & \boldsymbol{0}_3 & -\hat{\boldsymbol{R}}_b^n & -\hat{\boldsymbol{R}}_b^n \boldsymbol{S}(\hat{\boldsymbol{f}}) & \boldsymbol{0}_3 \\ \boldsymbol{0}_3 & \boldsymbol{0}_3 & \boldsymbol{0}_3 & \boldsymbol{0}_3 & \boldsymbol{0}_3 \\ \boldsymbol{0}_3 & \boldsymbol{0}_3 & \boldsymbol{0}_3 & -\boldsymbol{S}(\hat{\boldsymbol{\omega}}) & -\boldsymbol{I}_3 \\ \boldsymbol{0}_3 & \boldsymbol{0}_3 & \boldsymbol{0}_3 & \boldsymbol{0}_3 & \boldsymbol{0}_3 \end{bmatrix} \tag{27}$$

where $\boldsymbol{I}_n$ and $\boldsymbol{0}_n$ are the $n \times n$ identity- and zero matrices, $\hat{\boldsymbol{R}}_b^n = \boldsymbol{R}(\hat{\boldsymbol{q}}_b^n)$, $\hat{\boldsymbol{f}} = \boldsymbol{f} - \hat{\boldsymbol{b}}_a^n$ and $\hat{\boldsymbol{\omega}} = \boldsymbol{\omega} - \hat{\boldsymbol{b}}_g^n$

D. Correction of nominal states

The correction filter is outputting error states, $\delta \boldsymbol{x}$, based on the the measurement errors. The correction of the nominal states is done according with the equations (15)-(19), which is straight forward. The only exception is the attitude estimates, which utilizes (21), that is

$$\hat{\boldsymbol{q}}_b^{n\,+} = \hat{\boldsymbol{q}}_b^{n\,-} \otimes (\boldsymbol{a}_g)_q \tag{28}$$

where the superscript with plus and minus represents the corrected and uncorrected nominal states respectively. After correction, the error states are reset.

III. Reference vectors

The previous design with measurements of the transitional states is enough to estimate all states with decent accuracy. Augmenting the estimator with measurements of *reference vectors* will however further reduce the estimation error.

A reference vector is a vector that is measured in two systems, for instance $\boldsymbol{r}^n$ and $\boldsymbol{r}^b$. The rotation needed to make one of the vector equal the other, $\boldsymbol{R}_b^n$, gives information about the orientation between the two systems. This rotation is unfortunately ambiguous, with multiple combinations of attitude parameters constructing the same rotation. Because of the mentioned ambiguity and the fact that a rotation about the reference vector would not be observable, two different linearly independent reference vectors are needed for full observability of the attitude. Proof for this is provided in Appendix B

A. Measurement model

The tightly coupled approach to integrate the reference vector measurement into the navigation system would be to use a measurement model of the vector. The true and estimated relationship between the two vector measurements represented with quaternion attitude parameters are modeled as

$$\boldsymbol{r}^n = \boldsymbol{R}_{\hat{b}}^n \boldsymbol{R}_b^{\hat{b}} \boldsymbol{r}^b \tag{29}$$

$$\hat{\boldsymbol{r}}^n = \boldsymbol{R}_{\hat{b}}^n (\boldsymbol{r}^b - \tilde{\boldsymbol{r}}^b) \tag{30}$$

where system $\{\hat{b}\}$ is the computed body-system, separated from the real body system with the attitude error and defined as

$$\boldsymbol{r}^{\hat{b}} = \boldsymbol{R}(\delta \boldsymbol{q})\boldsymbol{r}^b \tag{31}$$

When subtracting the two model, the model for measured error becomes

$$\tilde{\boldsymbol{r}}^n = \boldsymbol{r}^n - \hat{\boldsymbol{r}}^n = \boldsymbol{R}_{\hat{b}}^n (\boldsymbol{R}_b^{\hat{b}} - \boldsymbol{I}_3)\boldsymbol{r}^b - \boldsymbol{R}_{\hat{b}}^n \tilde{\boldsymbol{r}}^b \tag{32}$$

Assuming that the attitude error is small, i.e. $\boldsymbol{a}_g \approx \boldsymbol{0}$, the small angle approximation $\boldsymbol{R}_b^{\hat{b}} = \boldsymbol{I}_3 + \boldsymbol{S}(\boldsymbol{a}_g)$ is valid. Using this on (32) results in

$$\tilde{\boldsymbol{r}}^n = -\boldsymbol{R}_{\hat{b}}^n \boldsymbol{S}(\boldsymbol{r}^b)\boldsymbol{a}_g - \boldsymbol{R}_{\hat{b}}^n \tilde{\boldsymbol{r}}^b \tag{33}$$

Linearizing (33) with respect to the estimator's state variables gives

$$\frac{d}{d\hat{\boldsymbol{x}}}\tilde{\boldsymbol{r}}^n = \boldsymbol{H}_r = \begin{bmatrix} \boldsymbol{0}_3 & \boldsymbol{0}_3 & \boldsymbol{0}_3 & -\boldsymbol{R}_{\hat{b}}^n \boldsymbol{S}(\hat{\boldsymbol{r}}^b) & \boldsymbol{0}_3 \end{bmatrix} \tag{34}$$

B. Error propagation from reference vectors into attitude

The attitude measurements from reference vectors are dependent on accurate measurements of the reference vectors in both reference frames. To make things easier to read, the vectors in this section will be coordinate free. This could be done as what reference frames are used have no impact on the magnitude of the attitude measurement error. Based on the work of [14], a model for the attitude measurement error $\delta \boldsymbol{q}$ could be derived, based on the two measurement errors of the reference vector, $\delta \boldsymbol{r}_N$ and $\delta \boldsymbol{r}_B$. The errors will defined as

$$\boldsymbol{q}_m := \boldsymbol{q}_b^n + \delta \boldsymbol{q} \tag{35}$$

$$\boldsymbol{r}_{N_m} := \boldsymbol{r} + \delta \boldsymbol{r}_N \tag{36}$$

$$\boldsymbol{r}_{B_m} := \boldsymbol{r} + \delta \boldsymbol{r}_B \tag{37}$$

where $\boldsymbol{r}_{N_m}$ is vector $\boldsymbol{r}$ measured in system $\{n\}$ and $\boldsymbol{r}_{B_m}$ is vector $\boldsymbol{r}$ measured in system $\{b\}$. The errors $\delta \boldsymbol{r}_N$ and $\delta \boldsymbol{r}_B$ are not considered correlated. It's important to note that $\boldsymbol{r}_{N_m}$ and $\boldsymbol{r}_{B_m}$ are two different vectors, separated by the difference in measurement error.

As the attitude of $\{b\}$ relative to $\{n\}$ could be represented by a rotation about the axis $\boldsymbol{\epsilon}_n = ((\boldsymbol{q}_b^n)_{\boldsymbol{\epsilon}})_{\text{norm}}$, the only components of $\delta \boldsymbol{r}_N$ and $\delta \boldsymbol{r}_B$ that affects the attitude error lies in the plane perpendicular to $\boldsymbol{\epsilon}_n$, as the parallel components are unaltered. Additionally, error that are parallel with the true reference vector, i.e. $(\boldsymbol{r})_{\text{norm}}\delta \boldsymbol{r}$, will not affect the direction of $\boldsymbol{r}_m$, meaning it will neither affect the measured

attitude. This means that the measurement error only has a single component contributing to the final attitude error, which is along the direction perpendicular to both $\boldsymbol{\epsilon}_n$ and $\boldsymbol{r}$. This direction is defined by

$$\boldsymbol{r}_\delta = \frac{\boldsymbol{r} \times \boldsymbol{\epsilon}_n}{||\boldsymbol{r}||} \tag{38}$$

Having defined the reference vector error components contributing the attitude error, the operator for extracting the contributing part from the error vector is defined as

$$(\delta \boldsymbol{r})_{contr} := \left|\left| \boldsymbol{r}_\delta \cdot \delta \boldsymbol{r} \right|\right| \tag{39}$$

The resulting attitude measurement error's standard deviation is a first order approximation based on uncorrelated errors between the two measurement of the reference vector

$$\sigma(\delta \boldsymbol{q}) \approx \frac{\sqrt{\sigma\left((\delta \boldsymbol{r}_N)_{contr}\right)^2 + \sigma\left((\delta \boldsymbol{r}_B)_{contr}\right)^2}}{||\boldsymbol{r} \times \boldsymbol{\epsilon}_n||} \tag{40}$$

C. Utilized reference vectors

The feasibility of each reference vector depends highly on the situation. A magnetometer might give measurements of good quality in a place where the magnetic field is stable, but horrible next to an electrical generator. [14] gives a good overview of mensurable vectors used to find heading and how the vector measurement errors propagates into attitude error. All reference vectors are assumed unbiased and with measurement noise, meaning that the sensor models are

$$\boldsymbol{r}_m = \boldsymbol{r} + \boldsymbol{w}_{m,r} \tag{41}$$

1) Specific Force: The specific force vector is dominated by the gravitational force in most situations. It therefore contains little information about the vehicle's heading attitude as the vector is unaffected by such rotations. The sensors used to measure specific force is the accelerometer for body-fixed specific force, differentiation of position/velocity measurements for acceleration in NED-frame and a known gravity vector.

2) Magnetic field: This magnetic field vector, $\boldsymbol{m}$, is measured by an magnetometer. It is a fairly stable vector when not in an environment polluted by electromagnetic (EM) noise. As it is easily disrupted, either by active or passive environmental disturbances or by the vehicle's own EM noise, it is not always reliable. The direction of the field vector depends on the operating environment's latitude, so the rotational axes observed by it varies.

The field vector is assumed known in the NED frame, and equal

$$\boldsymbol{m}^n = \begin{bmatrix} 13.5758 \\ 0.8132 \\ 50.0765 \end{bmatrix} \tag{42}$$

given in nT. Values are local to Trondheim, Norway, and found by using [15].

3) Body-fixed velocity: Using the likes of optical flow or Doppler radar it is possible to directly measure the velocity of the vehicle in body frame, $\boldsymbol{v}^b$. Combining this measurements with the Kalman filter's existing estimate of the velocity in NED (provided by GNSS or UWB), $\boldsymbol{v}^n$, gives a usable reference vector. The requirements for this to work is notable visual gradients in the environment for the optical flow to detect, or a suitable environment for radar reflections.

IV. Case Studies

Four different cases have been simulated with the Monte Carlo method. The first is the reference flight, with a standard outfit of GNSS- and magnetometer-aiding. The next will deal with the case when GNSS and the magnetometer becomes unavailable during flight. These cases are meant to mimic scenarios where a UAV drone enter an environment where some measurements no longer are reliable. The algorithms for when said measurements should be discarded are topics for further work. All simulations are done with motion guaranteeing observable velocity- and acceleration vector. Results for each case is averaged over 100 different simulations.

A. Implementation

The motion made by the simulated multicopter UAV was created by implementing a reference following autopilot, based on the work in [12]. The reference path was constructed by adding several sine- and cosine waves on top of each other in order to guarantee persistent excitation of velocity and acceleration. The reference path was then low-pass filtered to avoid high frequency movements and discontinuous reference velocities. The true path can be seen in Figure 2.

The vectors for process- and measurement noise, $\boldsymbol{v}$ and $\boldsymbol{w}$, are

$$\boldsymbol{w} = \begin{bmatrix} \boldsymbol{w}_a^T & \boldsymbol{w}_{b,a}^T & \boldsymbol{w}_g^T & \boldsymbol{w}_{b,g}^T \end{bmatrix}^T \tag{43}$$

$$\begin{aligned} \boldsymbol{w}_a &= \begin{bmatrix} 2.0 \cdot 10^{-4} \\ 2.0 \cdot 10^{-4} \\ 2.0 \cdot 10^{-4} \end{bmatrix}, \boldsymbol{w}_{b,a} = \begin{bmatrix} 3.6 \cdot 10^{-9} \\ 3.6 \cdot 10^{-9} \\ 3.6 \cdot 10^{-9} \end{bmatrix} \\ \boldsymbol{w}_g &= \begin{bmatrix} 4.4 \cdot 10^{-5} \\ 4.4 \cdot 10^{-5} \\ 4.4 \cdot 10^{-5} \end{bmatrix}, \boldsymbol{w}_{b,g} = \begin{bmatrix} 1.2 \cdot 10^{-6} \\ 1.2 \cdot 10^{-6} \\ 1.2 \cdot 10^{-6} \end{bmatrix} \end{aligned} \tag{44}$$

$$\boldsymbol{v} = \begin{bmatrix} \boldsymbol{v}_p^T & \boldsymbol{v}_v^T & \boldsymbol{v}_m^T & \boldsymbol{v}_{v^b}^T \end{bmatrix}^T \tag{45}$$

$$\begin{aligned} \boldsymbol{v}_p &= \begin{bmatrix} 0.050 \\ 0.050 \\ 0.130 \end{bmatrix}, \quad \boldsymbol{v}_v = \begin{bmatrix} 0.010 \\ 0.010 \\ 0.030 \end{bmatrix} \\ \boldsymbol{v}_m &= \begin{bmatrix} 0.138 \\ 0.089 \\ 0.165 \end{bmatrix}, \boldsymbol{v}_{v^b} = \begin{bmatrix} 0.200 \\ 0.200 \\ 0.200 \end{bmatrix} \end{aligned} \tag{46}$$

The implementation of sensors dropping out were done by the respective measurements from the measurement vector $\boldsymbol{y}$ and their measurement noise covariances from $\boldsymbol{R} := \mathrm{cov}[\boldsymbol{v}]$

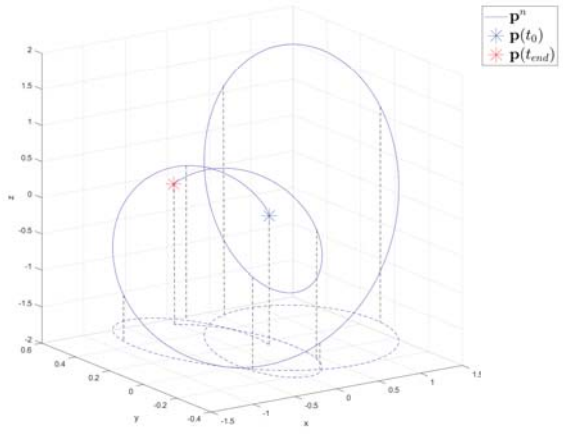

Fig. 2. 3D-view of the UAV's path, showing the path (blue, solid), a 2D projection of the path (blue, dashed), start and end points (blue and red star) and projection lines (black, dashed)

B. Results

1) Case 1: Flying with aiding from GNSS and magnetometer: The navigation results from reference flight yielded estimates with very low errors. The fusion of sensor information from many complementary sensors resulted in complete observability of all states, with only the relative low sensor sensor measurement noises to cause estimation errors. The only state that struggled to converge was the acceleration bias in the y direction, as can be seen in Figure 3. Notice also that the estimates of both $\boldsymbol{b}_a^b$ in Figure 4 and the attitude in Figure 5 are much less accurate than that of $\boldsymbol{b}_g^b$. This is likely due to the estimators inability to separate them as error sources due to lack of required rotation and acceleration. The estimation error numbers is found in Table I.

2) Case 2: Drop-out of Doppler-velocity and magnetometer: This case is representing the case when a UAV goes from an open outdoor environment to a place where the signals from GNSS and magnetometers are to unreliable to use. The vehicle is then only receiving aiding from UWB beacons for position measurements and otherwise maneuvering based on inertial navigation. The effects sets in at $t = 100$.

In Figure 6, the effects on the attitude estimation error could be seen. Quite naturally, it is the attitude and the velocity suffers the most from the sensor measurement drop-outs. However, the estimation for the x and y components is also worsening, with the y component completely unable to converge. The position estimates goes from an accuracy of several millimeters to a few centimeters, but is much less affected than the other states. The gyro-bias estimates is still tracking their true values, but with a further time lag than before the fall out. The change in estimation error variances could be seen in Table I.

3) Case 3: Drop-out, with aiding from body-velocity measurements: In this case it is tried to add an additional measurement source to the navigation system as an attempt to improve the estimate accuracy in the absence of reliable magnetometer measurements. It is taken into account that some indoor areas could have a plain and feature-less environment with few strong features for an optical sensor to track. The body-velocity measurements are therefore given large measurement noise, with a standard deviation of 20 cm in all directions. As this equals to about 10 % of the maximum velocity during the flight, there is no expectation that these measurements will have an equally positive effect as the magnetometer.

From a single simulation, there is no obvious improvement from Case 2. However, when inspecting the results from the Monte Carlo simulation in Table I, its clear that some improvements were achieved. Most notably is the improvement in heading accuracy, which goes from 3.70° to 2.78°, an error decrease of about 25 %.

4) Case 4: Drop-out, with aiding from specific force: This is perhaps the most interesting case. While an estimation of the specific force is necessary in nonlinear observers such as in [9], estimating it and using it to augment the Kalman filter estimation makes no improvement at all. The results is not even included as they are, on average, identical to when the reference vector is not used.

The vehicle acceleration in NED-frame, $\boldsymbol{a}^n$, is estimated by applying a separate Kalman filter, that uses solely the position and velocity measurements. This is done to avoid the estimation errors from both acceleration biases and the attitude to enter the filter. As the measurement noise used for integrating the acceleration estimate into the original Kalman filter, the error variance estimate (the diagonals of $\boldsymbol{P}$) of the acceleration states from the secondary Kalman filter is used.

The reason for lack of improvement using the specific force as a reference vector is likely because it provides no new information. The sensors involved in estimating the vectors in both frames are already used in the original Kalman filter. Looking at Equation 2, it is clear that a comparison between $\boldsymbol{f}^n$ and $\boldsymbol{f}^b$ is done in the model.

TABLE I
TABLE SHOWING THE RESULTS FROM THE MONTE CARLO SIMULATIONS OVER AVERAGE ESTIMATION ERRORS

	Case 1	Case 2	Case 3
$\delta\psi - \sigma$	0.44°	3.70°	2.78°
$(\delta\phi, \delta\theta) - \sigma$	0.12°	0.81°	0.70°
$\delta\boldsymbol{v} - \sigma$	$1.2\frac{cm}{s}$	$7.5\frac{cm}{s}$	$6.6\frac{cm}{s}$
$\delta\boldsymbol{p} - \sigma$	$1.9cm$	$2.9cm$	$2.8cm$

V. CONCLUSION

This paper has looked into a navigation solution that improves state estimation accuracy in GNSS- and magnetometer denied environments, given suitable motion of the vehicle. A simulator Monte Carlo simulations of four different cases comparing estimation accuracy of different sensor measurements show that even using velocity as a noisy reference vector improves heading estimates by 25 % in the case of GNSS and magnetometer dropout. It also had a notable

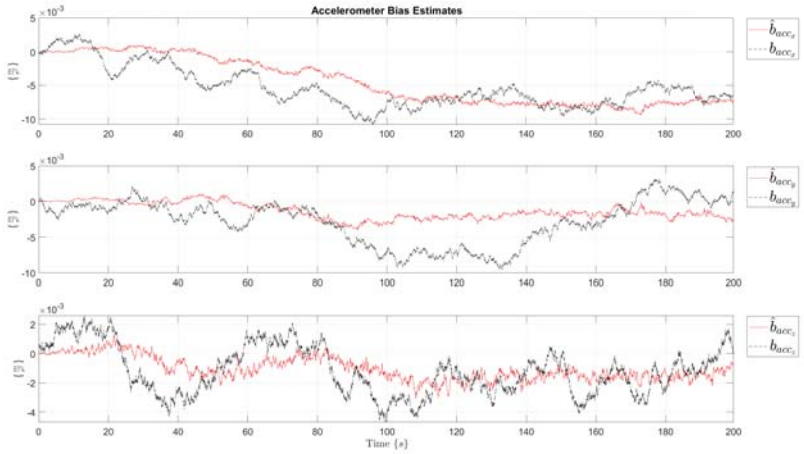

Fig. 3. Plots showing the acceleration bias estimates and the true values for Case 1.

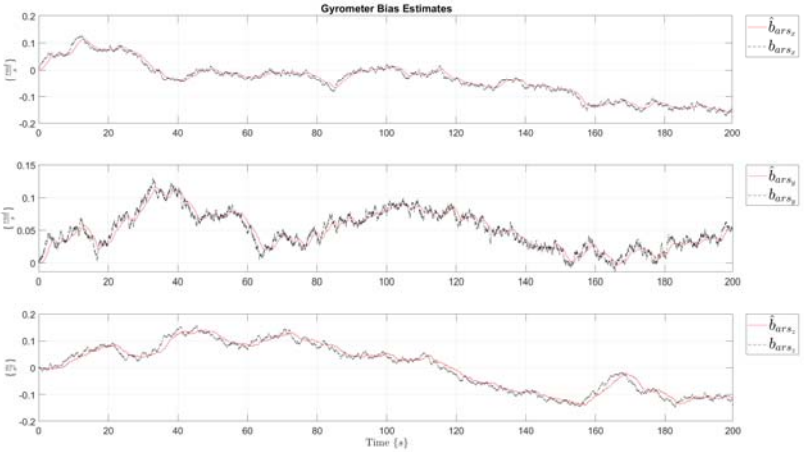

Fig. 4. Plots showing the gyro-bias estimates and the true values for Case 1.

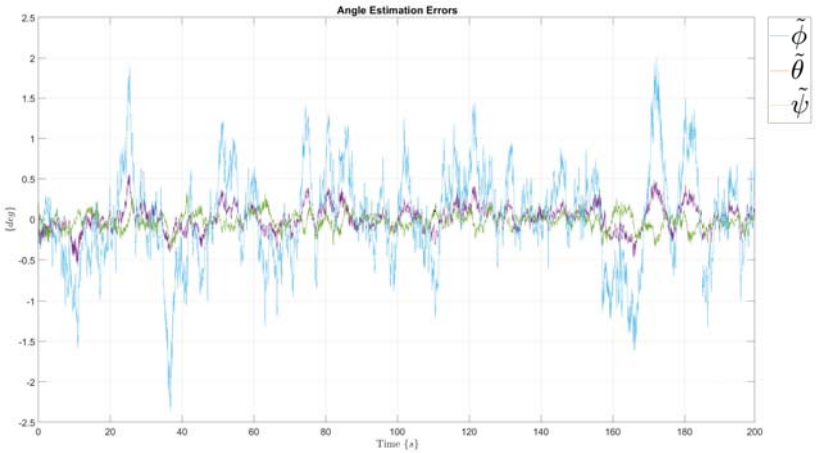

Fig. 5. Plots showing the attitude estimation errors for Case 1. Due to readability, it is represented in Euler angles.

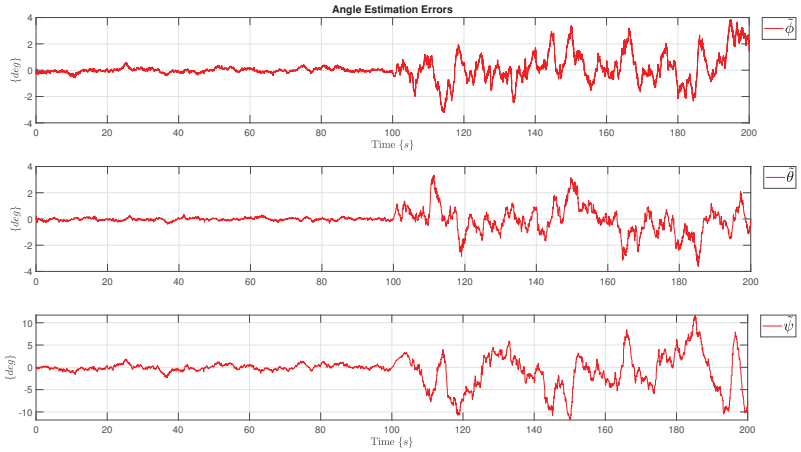

Fig. 6. Plots showing the attitude estimation errors for Case 2.

positive effect on the estimates velocity state, roll- and pitch angle, even though not as great as for heading. Position estimates is about unchanged, which is to be expected as position measurements are still available. Using specific force as a reference vector had next to no impact on accuracy at all. It is a likely speculation that this is because this reference vector is already integrated into the navigation model.

APPENDIX

A. System Observability

For the navigation system equations to converge, all states need to be observable. For this, the previously mentioned position- and velocity measurements are combined attitude measurements. They are handled as loosely coupled measurements while in reality being tightly, but that simplification is justified in Section B. Observability without direct attitude measurements is also possible, but require specific motion that is discussed in [16]

Using theory from [17, Chap. 6], the following theorem proves local observability:

Let $\boldsymbol{A}(t) \in \mathbb{R}^{n\times n}$ and $\boldsymbol{C}(t) \in \mathbb{R}^{m\times n}$ be C^{n-1}. Then the pair $(\boldsymbol{A}(t), \boldsymbol{C}(t))$ is observable at t_0 if there exists a finite $t_1 > t_0$ such that

$$rank \begin{bmatrix} \boldsymbol{N}_1(t_1) \\ \boldsymbol{N}_2(t_1) \\ \vdots \\ \boldsymbol{N}_n(t_1) \end{bmatrix} = n \tag{47}$$

where

$$\boldsymbol{N}_{i+1}(t) = \boldsymbol{N}_i(t)\boldsymbol{A}(t) + \dot{\boldsymbol{N}}_i(t), \quad i = 1, 2 \ldots, n-1 \tag{48}$$

with

$$\boldsymbol{N}_1 = \boldsymbol{C}(t) \tag{49}$$

With a slight change of notation, we use

$$\boldsymbol{C}(t) = \boldsymbol{H}(t) = \begin{bmatrix} \boldsymbol{I}_3 & \boldsymbol{0}_3 & \boldsymbol{0}_3 & \boldsymbol{0}_3 & \boldsymbol{0}_3 \\ \boldsymbol{0}_3 & \boldsymbol{I}_3 & \boldsymbol{0}_3 & \boldsymbol{0}_3 & \boldsymbol{0}_3 \\ \boldsymbol{0}_3 & \boldsymbol{0}_3 & \boldsymbol{0}_3 & \boldsymbol{I}_3 & \boldsymbol{0}_3 \end{bmatrix} \tag{50}$$

and that $\boldsymbol{A}(t) = \boldsymbol{F}$, where all the elements of $\boldsymbol{F}$ is known at time t as they build upon previous estimates. This gives that

$$\boldsymbol{N}_o(t) = \begin{bmatrix} \boldsymbol{N}_1(t) \\ \boldsymbol{N}_2(t) \end{bmatrix} = \begin{bmatrix} \boldsymbol{I}_3 & \boldsymbol{0}_3 & \boldsymbol{0}_3 & \boldsymbol{0}_3 & \boldsymbol{0}_3 \\ \boldsymbol{0}_3 & \boldsymbol{I}_3 & \boldsymbol{0}_3 & \boldsymbol{0}_3 & \boldsymbol{0}_3 \\ \boldsymbol{0}_3 & \boldsymbol{0}_3 & \boldsymbol{0}_3 & \boldsymbol{I}_3 & \boldsymbol{0}_3 \\ \boldsymbol{0}_3 & \boldsymbol{I}_3 & \boldsymbol{0}_3 & \boldsymbol{0}_3 & \boldsymbol{0}_3 \\ \boldsymbol{0}_3 & \boldsymbol{0}_3 & -\hat{\boldsymbol{R}} & -\hat{\boldsymbol{R}}\boldsymbol{S}(\hat{f}^b) & \boldsymbol{0}_3 \\ \boldsymbol{0}_3 & \boldsymbol{0}_3 & \boldsymbol{0}_3 & -\boldsymbol{S}(\hat{\boldsymbol{\omega}}) & -\boldsymbol{I}_3 \end{bmatrix} \tag{51}$$

Using the fact that rotation matrices by definition has rank of 3, it is clear that $\boldsymbol{N}_o(t)$ has rank of $n = 15$, meaning that they system is at least locally observable.

B. Attitude Observability from reference vectors

In Section A, the attitude measurements are treated as being loosely coupled, while they in reality are tightly coupled in the form of reference vectors. It is however a reasonable simplification to use, as two or more reference vectors still provide full observability of the attitude.

Proof: The linearized measurement model for reference vectors shows only one non-zero element, that is $\frac{d}{d\boldsymbol{a}}\tilde{\boldsymbol{r}}^n = -\boldsymbol{R}^n_{\hat{b}}\boldsymbol{S}(\hat{\boldsymbol{r}}^b)$. As this matrix is a known rotation of a skew-symmetric matrix, the rank will be the same as the rank of the skew-symmetric matrix. To find the rank of $\boldsymbol{S}(\hat{\boldsymbol{r}}^b)$, its null-space will be inspected. The symbols $\boldsymbol{a}$ and $\boldsymbol{b}$ will for the observability analysis represent two arbitrary three-dimensional vectors. As the notation $\boldsymbol{S}(\boldsymbol{a})\boldsymbol{b}$ is the cross product between the two vectors, this product will only give the null-vector when $\boldsymbol{a} \parallel \boldsymbol{b}$, meaning that the null-space of $\boldsymbol{S}(\boldsymbol{a})$ is one-dimensional and that the matrix' is of rank 2. The attitude of any 3-D rigid body has three degrees of freedom, meaning that an observability matrix from a single reference vector insufficient to observe the complete attitude.

When another reference vector is introduced, the measurement vector's observation of the attitude turns into

$$\frac{d}{d\boldsymbol{a}}\boldsymbol{h}(\boldsymbol{x}) = \frac{d}{d\boldsymbol{a}}\begin{bmatrix}\tilde{\boldsymbol{r}}_1^n \\ \tilde{\boldsymbol{r}}_2^n\end{bmatrix} = \begin{bmatrix}-\boldsymbol{R}_b^n \boldsymbol{S}(\hat{\boldsymbol{r}}_1^b) \\ -\boldsymbol{R}_b^n \boldsymbol{S}(\hat{\boldsymbol{r}}_2^b)\end{bmatrix} \tag{52}$$

As the rotation is irrelevant for the rank of this matrix, it will be omitted further observability analysis, and we define

$$\boldsymbol{H}_r = \begin{bmatrix}\boldsymbol{S}(\hat{\boldsymbol{r}}_1^b) \\ \boldsymbol{S}(\hat{\boldsymbol{r}}_2^b)\end{bmatrix} \tag{53}$$

where $\boldsymbol{H}_r \in \mathbb{R}^{6\times 3}$

Again, the easiest way to find the rank of the matrix $\boldsymbol{H}_r$ is to inspect its null-space. It was previously stated that the only way that $\boldsymbol{S}(\hat{\boldsymbol{r}}_1^b)\boldsymbol{a} = \vec{0}$ is if $\hat{\boldsymbol{r}}_1 \parallel \boldsymbol{a}$. Subjecting the matrix $\boldsymbol{H}_r$ to the same conditions, it shows that $\boldsymbol{H}_r\boldsymbol{a} = \vec{0}$ if and only if $\boldsymbol{a} \parallel \hat{\boldsymbol{r}}_1$ and $\boldsymbol{a} \parallel \hat{\boldsymbol{r}}_2$, implying that $\hat{\boldsymbol{r}}_1 \parallel \hat{\boldsymbol{r}}_2$. If the two reference vectors are to be non-parallel, in other words linearly independent, then $\boldsymbol{H}_r$ would have an empty null-space and a guaranteed rank of 3, giving full observability of the attitude.

REFERENCES

[1] Gérard Lachapelle et al. GNSS indoor location technologies. *Journal of Global Positioning Systems*, 3(1-2):2–11, 2004.

[2] Janis Tiemann, Florian Schweikowski, and Christian Wietfeld. Design of an UWB indoor-positioning system for UAV navigation in GNSS-denied environments. In *2015 International Conference on Indoor Positioning and Indoor Navigation (IPIN)*, pages 1–7, Oct 2015.

[3] Kristoffer Gryte, Jakob M. Hansen, Tor A. Johansen, and Thor I. Fossen. Robust navigation of UAV using inertial sensors aided by UWB and RTK GPS. *AIAA Guidance, Navigation, and Control Conference*, 2017.

[4] Rongbing Li et al. LIDAR/MEMS IMU integrated navigation (SLAM) method for a small UAV in indoor environments. In *2014 DGON Inertial Sensors and Systems (ISS)*, pages 1–15, Sept 2014.

[5] Brita Helene Hafskjold, Bjørn Jalving, Per Espen Hagen, and Kenneth Gade. Integrated camera-based navigation. *Journal of Navigation*, 53(2):237245, 2000.

[6] Baheerathan Sivalingam and Ove Kent Hagen. Image-aided inertial navigation for an octocopter. page 20, 05 2018.

[7] Rudolf E Kalman. A new approach to linear filtering and prediction problems. *Transactions of the ASME*, 82(1), 1960.

[8] F. Landis Markley. Attitude error representation for kalman filtering. *Journal of Guidance, Control, and Dynamics*, 2003.

[9] Håvard F. Grip, Thor I. Fossen, Tor A. Johansen, and Ali Saberi. Globally exponentially stable attitude and gyro bias estimation with application to GNSS/INS integration. *Automatica*, 2015.

[10] Tor A. Johansen and Thor I. Fossen. Nonlinear observer for tightly coupled integration of pseudorange and inertial measurements. *IEEE Transaction on Control Systems Technology*, 2016.

[11] Tor A. Johansen and Thor I. Fossen. The eXogenous Kalman filter (XKF). *International Journal of Control*, 90(2):161–167, 2017.

[12] Kristian Klausen, I. Fossen, Thor, and Tor A. Johansen. Nonlinear control of a multirotor UAV with suspended load. In *2015 International Conference on Unmanned Aircraft Systems (ICUAS)*, pages 176–184, June 2015.

[13] Elliot D. Kaplan and Christopher J. Hegarty. *Understanding GPS/GNSS: Principles and Applications*. Artech House, 2017.

[14] Kenneth Gade. The seven ways to find heading. *Journal of Navigation*, 69(5):955–970, 2016.

[15] National Center of Environmental Information. Magnetic field calculator, 2018. https://www.ngdc.noaa.gov/geomag-web/#igrfwmm [Accessed 2018-11-20].

[16] Paul Groves. *Principles of GNSS, Inertial, and Multisensor Integrated Navigation Systems*. Artech House, 2013.

[17] Chi-Tsong Chen. *Linear System Theory and Design*. Oxford Univercity press, 2013.